Femtosecond laser tagging in 1,1,1,2-Tetrafluoroethane with trace quantities of air

Yibin Zhang,* and Richard B. Miles†
Princeton University, Princeton, NJ, 08544, USA
Paul M. Danehy,‡
NASA Langley Research Center, Hampton, VA 23666

Femtosecond laser tagging is demonstrated for the first time in R134a gas, and in mixtures of R134a with small quantities of air. A systematic study of this tagging method is explored through the adjustment of gas pressure, mixture ratio and laser properties. It is found that the signal strength and lifetime are greatest at low pressures for excitation at both the 400 nm and 800 nm laser wavelengths. The relative intensities of two spectral peaks in the near-UV emission change as a function of gas pressure and can potentially be used for local pressure measurements. Single shot precision in pure R134a and R134a with 5% air is demonstrated at the exit of a subsonic pipe flow. The parameter space of these results are chosen to mimic conditions used in the NASA Langley Research Center's Transonic Dynamics Tunnel. The precision and signal lifetime demonstrate the feasibility of using this technique for measuring flowfields that induce airfoil flutter.

I. Introduction

A. NASA Transonic Dynamics Tunnel

The Transonic Dynamics Tunnel (TDT)[1–4] at the NASA Langley Research Center is a large-scale variable pressure closed-circuit wind tunnel capable of using 1,1,1,2-Tetrafluoroethane (CH_2FCF_3, R134a) or air at speeds up to Mach 1.12. R134a serves as a high density fluid for aeroelastic model testing. R12, a chlorofluorocarbon (CFC), was formerly used as the heavy gas test medium but ultimately phased out due to the enactment of the Montreal Protocol and U.S. Clean Air Act. In 1995, R134a was chosen as a more environmentally safe alternative to the other candidate gas, sulphurhexafluoride (SF6), and continues to be used today. The TDT Heavy Gas Reclamation System introduces the heavy gas into the tunnel prior to testing and evacuates it after the test through an air-to-heavy gas exchange detailed by Corliss.[2] This method typically leaves behind trace percentages of air in the heavy gas flow. The TDT has an octagonal cross section of 16 feet by 16 feet and supports the installation of a variety of mount systems including sting mounts, a sidewall turntable, a floor mounted turntable, a two-cable free-flight support system, helicopter test apparatuses, tilt-rotor test apparatuses and custom mount systems. A large matrix of observation windows provides optical access to the test section.

The motivations for testing in TDT are closely coupled with the complexities that arise in the transonic flow regime. Transonic flow is a mixture of sub- and supersonic local flow with nonlinear flow features introduced by the presence of oscillating shocks. When the maximum local velocity on an airfoil in the flow becomes supersonic, a shock develops and moves along the surface, leading to rapid variations in drag, lift and pitching as the Mach number changes. Aeroelasticity, the interplay of structural (elastic, inertial) and aerodynamic forces, is responsible for a number of dynamic behaviors such as limit cycle oscillations (LCO), internal resonances and chaotic motion,[5] as well as for static phenomena such as deformation of aircraft parts under aerodynamic loads. The unsteady aerodynamics of airfoils and wings in transonic flow create

*Graduate Student, Department of Mechanical and Aerospace Engineering, Princeton, AIAA Student Member
†Robert Porter Patterson Professor Emeritus, Department of Mechanical and Aerospace Engineering, Princeton, AIAA Fellow
‡Senior Technologist for Advanced Measurement Systems, NASA Langley Research Center, Hampton, VA 23666

a phenomenon called "flutter", or oscillatory instabilities that can lead to catastrophic failure of the part if not mitigated. Over the past few decades, the TDT has frequently been used for studying flutter trends, nonlinear transonic effects on flutter, aeroelastic characteristics of different wing and rotor concepts and active control methods, as well as for providing CFD model validation. NASA Langley's TDT has played a large role in the development of active controls technology by providing a facility for testing new concepts and validating models and design methods. In addition to aeroelasticity programs, the TDT has been used for space-related test programs that take advantage of its large test section, variable pressure capabilities and heavy gas medium.[4] These tests address launch vehicle and spacecraft transition through Earth and similar atmospheres, launch vehicle ground-wind loading due to the natural wind environment, launch vehicle dynamics, atmospheric flight, atmospheric reentry, and effects of planetary conditions on instrumentation accuracy during landing.

Critical to the objective of the TDT wind tunnel test program is the validation of flutter suppression techniques[6,7] and the ability to assess the effectiveness of active controls. The program aims to understand and predict nonlinear dynamic response behaviors of the aircraft in order to improve overall reliability, safety and performance. To validate these methods and theories, measurements of local flow are required. A robust diagnostic method with high spatial and temporal resolution is needed to measure local flow behaviors under transonic conditions in mixtures of R134a with small percentages of air.

B. Laser velocimetry tagging

Probe- and sensor-based diagnostics are intrinsically intrusive and unable to provide accurate measurements of difficult flow features, such as small scale structures and boundary layer fluctuations, without changing the flowfield of interest. Recent developments towards less-intrusive fluid diagnostics include pressure- and temperature-sensitive paints for making surface measurements,[8–10] Rayleigh scattering velocimetry,[11] laser-induced thermal acoustics,[12] and Laser Doppler anemometry,[13] the latter which was applied to study freestream velocity fluctuations in the NASA Langley 0.3-meter Transonic Cryogenic Tunnel. Unseeded, laser-based velocimetry methods are becoming increasingly popular as a result of improvements in laser technology and increased demand for more robust gas diagnostics in high speed test facilities. A number of methods, including scattering techniques and ozone tagging, take advantage of existing particles in the air to produce measurable signals from a distance. These are advantageous compared to their seeded counterparts since homogeneous seeding is difficult to accomplish and the presence of particles may alter the flowfield. Molecular tagging methods with a signal lifetime that is long compared to the flow convection timescale are especially desirable in air-breathing testing facilities that mimic aircraft flight conditions. Current techniques in air include VENOM[14] (vibrationally-excited nitric oxide monitoring), RELIEF[15] (Raman excitation and laser induced electronic fluorescence), and APART[16] (air photolysis and recombination tracking), to name a few.

The current study focuses on a variation of the Femtosecond Laser Electronic Excitation Tagging technique. Femtosecond Laser Electronic Excitation Tagging (FLEET) is a laser diagnostic method for velocimetry with the necessary spatial and temporal resolution for low- through high-speed flows.[17] The visible FLEET emission is produced as a result of the ionization, dissociation and recombination processes following femtosecond laser excitation of nitrogen-containing gases. The main emission contributor is the nitrogen first positive system, the transition from the nitrogen B electronic state to the A state. This emission, the Lewis-Rayleigh afterglow, is a visible fluorescence that is swept with the flow and can be tracked with a camera to give velocity and acceleration. Ultrafast laser pulses have intensities that are orders of magnitude higher than their nanosecond equal-energy counterparts, and femtosecond pulses in particular have a pulse duration that is much shorter than the collision time at atmospheric conditions. Because of this, breakdown processes do not need to be considered in the excitation physics.

FLEET has previously been used to measure the flowfield around a symmetric airfoil in the NASA Langley 0.3-m Transonic Cryogenic Tunnel, a closed-loop fan-driven wind tunnel operating at subsonic conditions with nitrogen working gas.[18] Recently a resonant version of this process, called Selective Two-Photon Absorptive Resonance FLEET (STARFLEET) has been developed.[19] STARFLEET uses over an order of magnitude lower pulse energy at the same laser repetition rate for tagging (1 kHz), at the cost of increasing the optical setup complexity because it relies on producing and transmitting UV wavelengths. Improvements in the frequency response (up to 100 kHz) of these nitrogen tagging velocimetry methods have also been made with the use of a picosecond laser instead of a femtosecond laser, resulting in a technique called Picosecond Laser Electronic Excitation Tagging (PLEET).[20] Femtosecond laser excitation for velocimetry has been

studied in a number of different gaseous mixtures, including oxygen, argon, carbon dioxide and methane, and notable lifetimes have been measured in all but methane gas.[21–23] The mechanisms at work are expected to be vastly different for tagging in single-gas species or air versus in pure R134a. Femtosecond laser near-infrared interactions of polyatomic molecules composed of carbon, hydrogen, and halogen group atoms result primarily in dissociation through field ionization and fragmentation. Formation of CF_4, CF_3H and secondary product CF_2 is expected.[24] The fluorescence lifetime and decay of gaseous 1,1,1,2-Tetrafluoroethane following femtosecond laser multiphoton ionization and dissociation has not previously been explored, to the best of the authors' knowledge.

II. Experiment

We investigate the possibility of extending femtosecond laser tagging to flows composed primarily of gaseous R134a for application in the NASA TDT. Tests are conducted in a glass cylindrical gas cell ($d \approx 2$") with optically clear windows that allow $> 94\%$ transmission at the operating laser wavelengths, 800 nm and 400 nm. Mixtures of R134a and industrial-grade air are supplied from a gas-mixing manifold and flowed through the cell. A rotary vane vacuum pump evacuates the cell and helps to regulate pressure between 0.1 and 1.0 atmospheres. The laser used in this study is a Spectra Physics Solstice laser with titanium sapphire oscillator and MaiTai regenerative amplifier operating at a fundamental wavelength centered at 800 nm with 1 kHz repetition rate. Frequency-doubling to 400 nm is achieved with a SHG BBO crystal at approximately 30% efficiency. Focusing of the beam is performed with a f=25 cm focusing lens. We use an intensified CMOS PCO.dimax HD+ camera system with a 1920x1440 pixel resolution at 11 μm by 11 μm pixel size and maximum frame rate of 2128 frames per second to obtain both broad-spectrum images and spectra of the tagged line. An experimental spatial resolution of 18 μm per pixel is attained through the use of extension tubes. Signal amplification is achieved with a Quantum Leap gateable image intensifier module with a reported resolution of > 60 LP/mm and gate repetition rate of 2 MHz. The intensifier serves the dual purpose of signal amplification and high-speed shutter. The MCP gain is held constant for the duration of the experiment at approximately 8.3/10 to minimize amplification of background noise. Two lenses collimate and focus the diffuse radiating signal into the slit of an Acton SpectraPro 300i spectrometer for spectroscopy. The intensity and lifetime of the visible emission at different mixtures and pressures is measured and reported on in this study. Intensity is determined by summing all the signal counts in a rectangular area enclosing the radiating line, and subtracting the same sum of background counts with no signal present. This process reduces the effect of shot-to-shot fluctuations in the gas flow.

The optically clear cylindrical gas cell is depicted in Figure 1. It is supported by two sets of clamps and the laser beam is focused into the center of the cell. These two photographs depict the emission as seen by the naked eye (or an ordinary DSLR camera) under different pressure conditions. At low pressures, the emission appears to be bright blue, and as the pressure is increased, it gradually becomes violet before turning white. These changes reflect the strong pressure sensitivity of this tagging process. Time-gated spectra, which are only resolvable within the first several hundred nanoseconds, are taken of the emitting line in order to give insight to the processes responsible for these changes.

Figure 2 depicts spectra that are temporally integrated over the first hundred nanoseconds following femtosecond laser excitation for two different pressure conditions. In the presence of small amounts of nitrogen ($\approx 20\%$ mole fraction), there are two prominent features around 350 and 430 nm that may be attributed to spectral lines in the C_2 Swan band or the $A^2\Delta - X^2\Pi$ and $B^2\Sigma - X^2\Pi$ transitions of the CH radical. Further fluorescence in the UV (from CF_2 and CF radicals) may contribute to the overall signal as well, but lie outside of the resolvable range of our spectroscopy equipment. No other detectable spectra are observed in the experiment. Time-integrated spectra in pure R134a or R134a + 15% air taken with a Princeton Instruments PIXIS 512B camera in combination with the spectrometer offered similar or worse resolution of intensity differences between the same two peaks at different pressures.

Figure 3 shows signal decay curves taken at different pressures for 15%Air + 85%R134a, which was chosen as the maximum air-to-R134a ratio expected to be encountered in the TDT. The signal is measured as the sum of the averaged intensity over 100 shots in a fixed region, indicated by the red boxes, minus the background levels. Visuals corresponding to 50 and 120 a.u. averaged signal levels are given on the right panel. At P=0.2 atm, the signal in pure R134a is 1/10 the strength of that in air and 1/50 the strength of that in nitrogen under the same laser properties and focusing, a trend also observed at other pressure levels. Together, Figures 2 and 3 suggest that while air does not seem to have a large effect on the emission process,

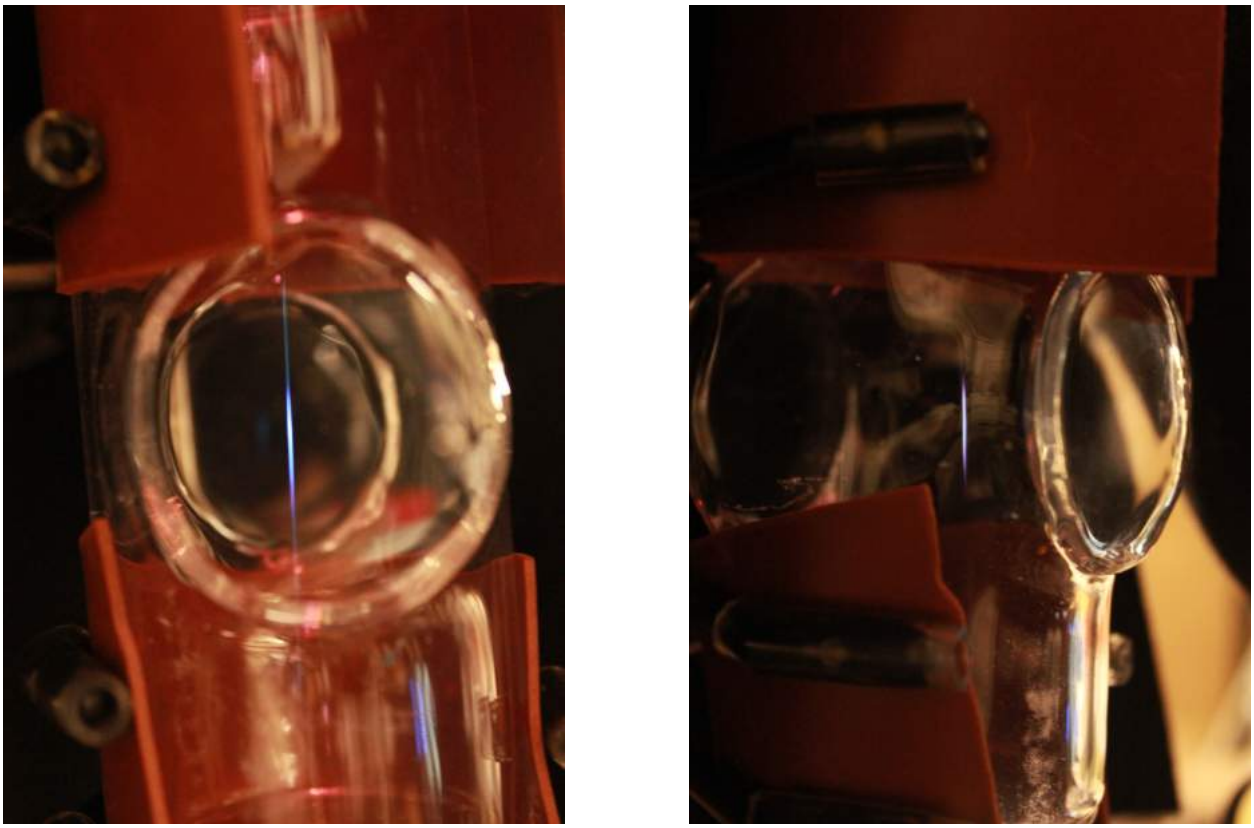

(a) P=0.07 atm (b) P=0.4 atm

Figure 1. Photographs of femtosecond laser excitation in 15% air + 85% (mole fraction) R134a at different pressures, taken with a Canon DSLR camera. At higher pressure levels (up to atmospheric), the emission appears white. Laser: $\lambda_c = 800$nm,1.5 mJ/pulse,1 kHz

the displacement of some freon molecules by air reduces the quenching of the radiation and thus allows for overall higher signal levels for most delays and pressure conditions.

Next, we determine that the minimum pulse energy necessary to produce visible emission in our gas cell at 800 nm and 1 kHz repetition rate with a f=25 cm focusing lens is 0.5 mJ. Figure 4a shows the signal decay curve for tagging with the minimum pulse energy at 0.7 atm and the corresponding averaged images. Figure 4b depicts single-shot images of the tagged line at 0.7 atm produced using pulse energies of 1.5 mJ and delays of $1, 3, 5\mu s$ (top row) and 0.5 mJ and delays of $0.5, 1, 3\mu s$ (bottom row).

The effects of pressure and delay on signal levels are studied in Figure 5. We observe that at low pressure conditions ($\lesssim 0.2$ atm), the signal strength and lifetime are strongest. Pressure appears to have the strongest effect on the measurable signal, second to delay time. Signals at longer delays and pressures $\gtrsim 0.5$ atm were not measurable with our experimental equipment. Delay time along the x-axis is the sum of the delay after pulse arrival plus half of the gate width.

Strong shot-to-shot fluctuations observed at low pressures (Figure 6) can be partially attributed to the limitations of our oil-sealed rotary vane pump. This type of pump creates a low pressure environment in the inlet connected to the test cell by mechanically trapping and compressing a volume of gas, and venting it through the exhaust outlet. An oil seal separates the inlet and outlet sides, as well as fills the gap between the rotor top and housing. At the high pumping speeds necessary to maintain a low-pressure environment, gas leakage around the seal can increase the signal fluctuations. We normalize these fluctuations with signal measurements in pure air to isolate and remove the effects of the vacuum pump on our signal. Another source of error comes from the individual gas flow-meters, which can oscillate and lead to slightly varying ratios between air and R134a especially in the third case (5% Air +95% R134a), which becomes more pronounced at low pressure levels. Measurements are made to show that these oscillations are relatively constant between the two flow-meters and their effects on the mean signal can be removed by averaging over many samples.

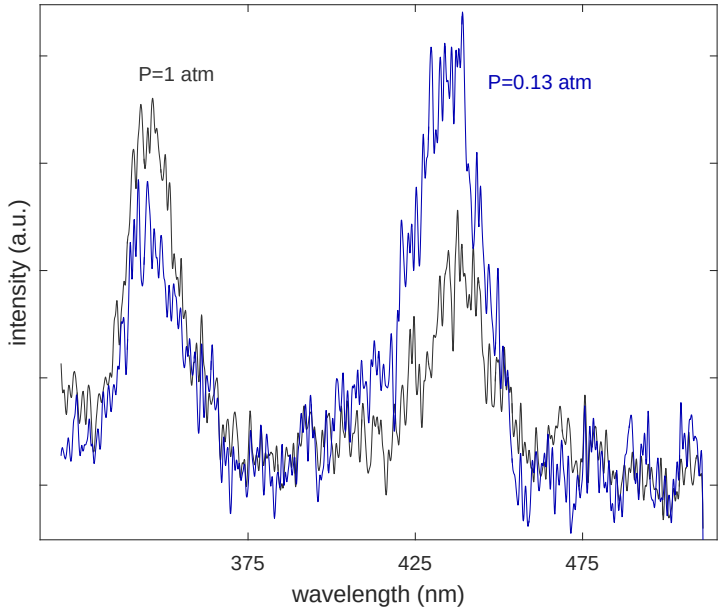

Figure 2. Spectra taken with $80\%R134a$ and $20\%N_2$, delay = 0 and 100 ns exposure. Laser: $\lambda_c = 800$ nm,1.5 mJ/pulse,1 kHz

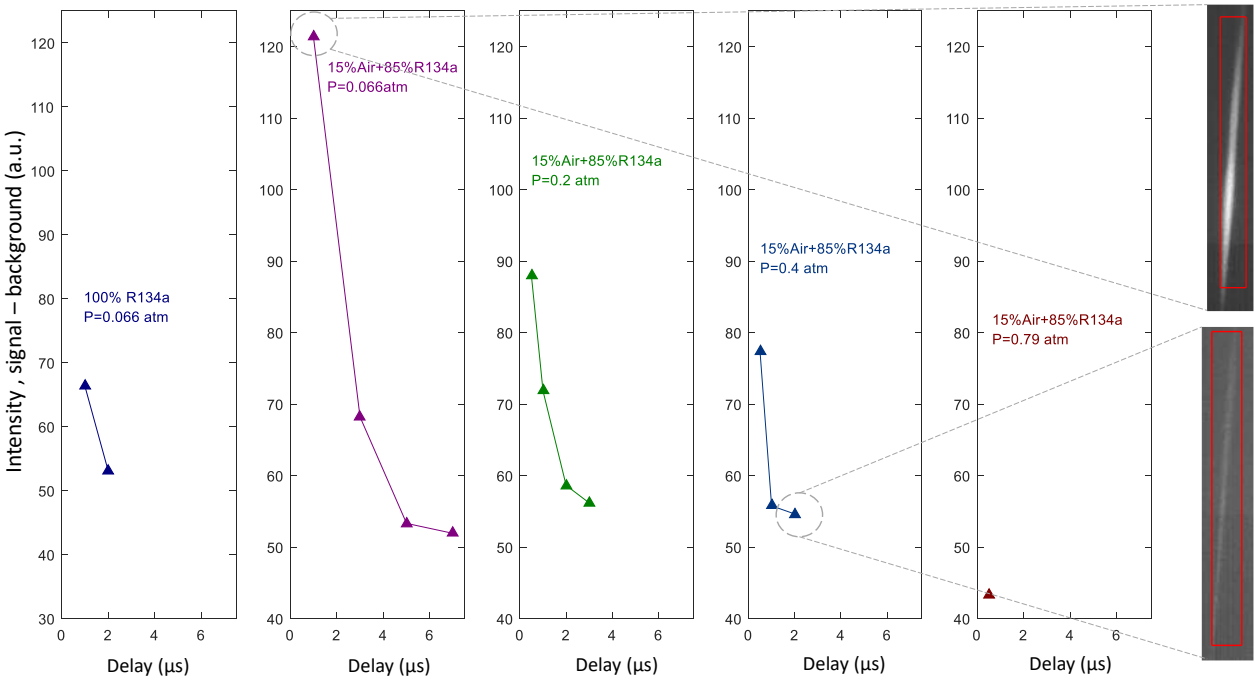

Figure 3. Signal decay curves for data averaged over 100 shots taken at different pressures, using a 1.5 mJ laser pulse centered at 800 nm. Note that the y-axis (signal intensity) does not begin at zero. On the right are two averaged representations of the signal at approximately 120 a.u. and 50 a.u.

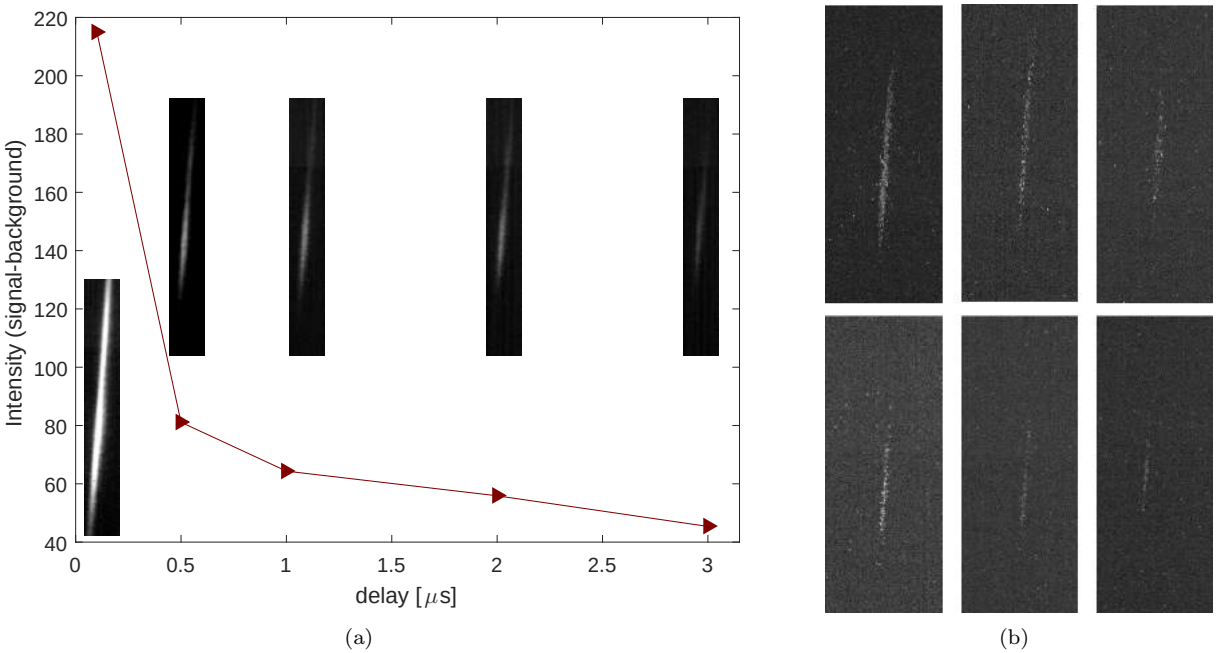

Figure 4. Signal at the minimum pulse energy needed for tagging in mixtures of 15%Air $+ 85\%$R134a. (a) Intensity at lowest pulse energy, 0.5 mJ, and 0.7 atm. (b) Single shot images of the signal at 0.7 atm. Top row: 800 nm, 1.5 mJ/pulse, $d = 1, 3, 5\mu s$. Bottom row: 800 nm, 0.5 mJ/pulse, $d = 0.5, 1, 3\mu s$

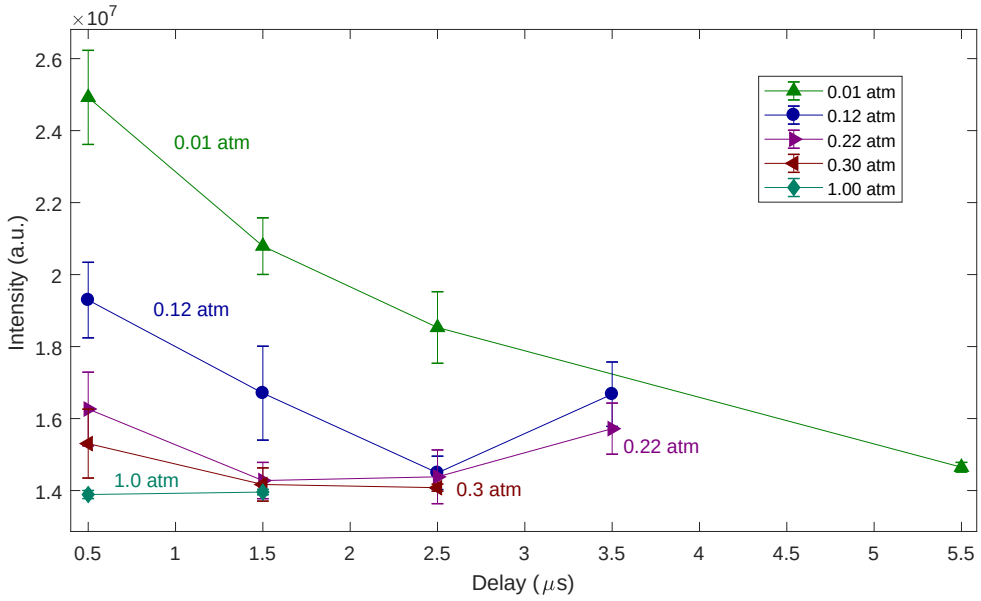

Figure 5. Emission intensity in pure R134a at different pressures and delays, where the delay, t, is defined by $t = d + \frac{1}{2}g$ and the gate width is $1\mu s$. Note that the y-axis (emission intensity) does not begin at zero. Laser: $\lambda_c = 400$ nm,1.2 mJ/pulse,1 kHz

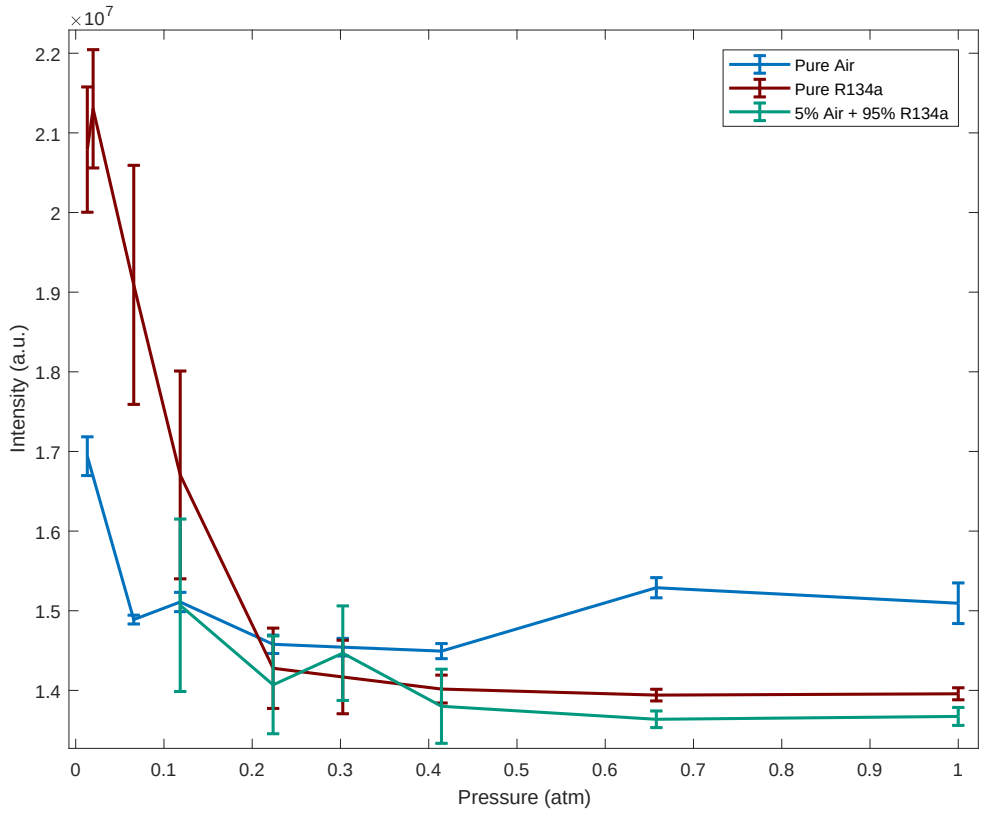

Figure 6. Signal intensity as a function of pressure for pure R134a and a R134a mixture with 5% air. The pure air line is plotted for comparison. Note that the y-axis (emission intensity) does not begin at zero. The delay is 2 μs and gate width is 1 μs. Laser: $\lambda_c = 400$ nm,1.2 mJ/pulse,1 kHz

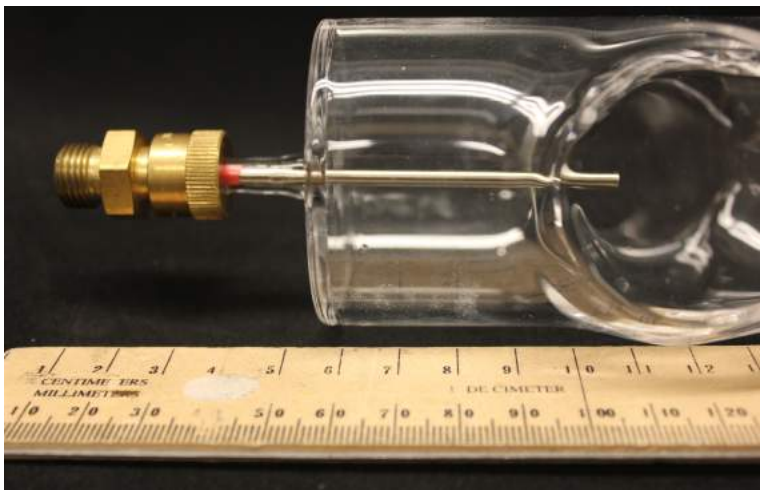

Figure 7. Gas cell modified with an inlet pipe insertion (⌀=2mm) for velocimetry

III. Single-shot precision

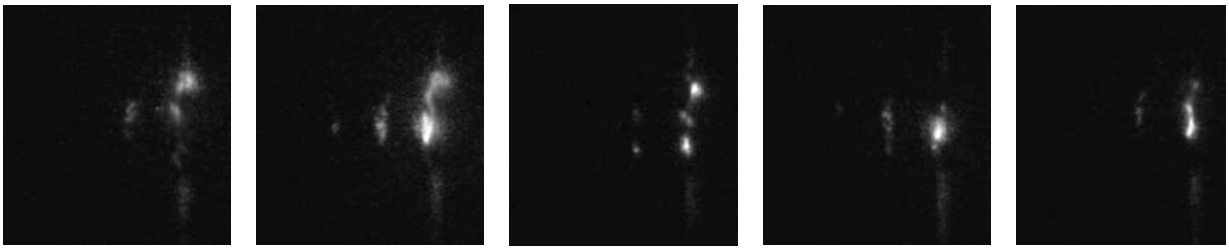

Figure 8. Single-shot images of femtosecond laser velocimetry in pure R134a flow at the pipe exit ($\varnothing = 2$mm, 230m/s), imaged in burst mode with camera delays at $t = 0, 5, 10\mu s$, gate of $0.5\mu s$. The flow is from right to left and each frame is about 6 mm across, horizontally. Each of the five frames depicts three exposures corresponding to the previously stated delays, $t = 0, 5, 10\mu s$. $t = 0$ corresponds to approximately 200ns following the pulse arrival time in order to temporally filter out Rayleigh scattering from the beam. The laser direction is from bottom to top of each frame. Laser: $\lambda_c = 800$ nm, 1.5 mJ/pulse, 1 kHz

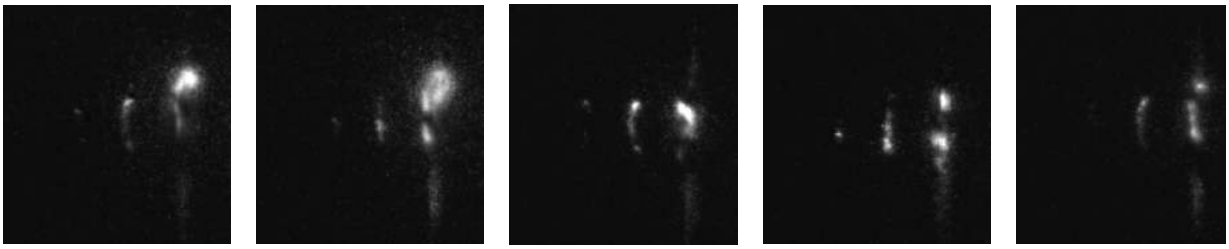

Figure 9. Single-shot images of femtosecond laser velocimetry in a mixed R134a + 5% air flow at the pipe exit, imaged in burst mode with camera delays at $t = 0, 5, 10\mu s$, gate of $0.5\mu s$. The optical arrangement and timing are the same as in Figure 8.

Figures 8 and 9 demonstrate velocimetry in a pipe flow as shown in the gas cell configuration (Figure 7). The pipe is long enough relative to its diameter such that the flow is fully-developed before rapidly expanding as it enters the evacuated cell. The laser pulse energy was increased to 3 mJ per pulse in this experiment to overcome losses as the focused beam enters the optical-grade fused silica flat windows on the cell located perpendicular to the cell's cylindrical axis, and the repetition rate is kept constant at 1 kHz. The laser beam is positioned normal to the pipe axis. The regulated supply pressure and measured gas cell pressure are close to 1 atmosphere, but that value is expected to deviate from the pressure seen by the laser signal at the pipe exit due to the pressure increase in the narrow pipe. $Re_D = 1.7 * 10^5$, which exceeds the critical Reynolds number for transition to turbulence in a pipe flow, so the flow is fully-developed and turbulent. Gas flow velocity is maximized so that a clear signal displacement could be measured in the cell. Three positions marked by the displaced emission captured in burst mode can be seen in some of the panels, demonstrating the capability for capturing small fluctuations in the flow with good temporal resolution. The first and longest signal line corresponds to the $t = 0$ delay (approximately 200ns following the pulse arrival time), imaged right after the Rayleigh scattering of the laser pulse; some bright scattering from the pipe is visible. In the second "burst" signal lines, we observe some uneven "clumping" of the emission that is

not seen in femtosecond laser tagging in diatomic or atomic gas mixtures. The positions of these "clumps" can potentially be used to resolve multiple components of velocity. In this study, no significant difference is observed between tagging in pure R134a or in a mixture with small percentages of air. We also notice that the increase in laser power corresponds to a longer lifetime, but care must be taken to balance the lifetime and strength of the signal with perturbations introduced by the deposited pulse energy. We find that in R134a tagging, the CMOS sensor frequently suffers from negative ghosting where depleted signal count regions occur following a high intensity event. Depleted signal counts typically fall between 5% and 70% of the average background signal. Approximately 2% of the images are strongly affected by this negative ghosting and these images are discarded for the subsequent velocity measurements.

A. Measurement Uncertainty

Errors in the displacement measurements may stem from three sources: the experimental apparatus, experimental conditions and data processing. Specifically, experimental apparatus error is frequently caused by the amplification of background noise by the intensifier. The intensifier module is found to enhance the digital count differences among the four quadrants of the camera's sensor, forming striations in the background image that are not generally visible under normal light conditions, but can nevertheless reduce signal quality. A flat-field correction is applied by dividing images by a map of sensitivity variations across the CCD and removing voltage bias through background subtraction. Uncertainties in the data processing step can be attributed to the fitting procedure. Because the displacement variation is much larger than any variations in the initial line position, we approximate the measurement uncertainty only as a function of final line position and timing uncertainty. Jitter from the laser trigger pulse to the camera is less than a nanosecond and can be safely disregarded, while timing errors introduced by the signal generation system has an upper limit of 35ns due to the length of the cables. The scale factor for the images is calibrated by imaging a ruler. Uncertainties in determining the pixel resolution result in errors of up to 3 microns per pixel and is accounted for in the overall displacement error calculation. Error in the velocity calculation can be derived from the general equation for uncertainty propagation for some function y that is dependent on variables $x_1, x_2, ..., x_n$ (Equation 1).[25] Equation 2 describes velocity uncertainty from measurement uncertainties in the initial line position x_0, final line position x_f, and timing Δt.

$$y = f(x_1, x_2, ..., x_n)$$

$$\Delta y = \sqrt{\left(\frac{\delta f}{\delta x_1}\Delta x_1\right)^2 + \left(\frac{\delta f}{\delta x_2}\Delta x_2\right)^2 + ... + \left(\frac{\delta f}{\delta x_n}\Delta x_n\right)^2} \quad [1]$$

$$V = f(\Delta x, \Delta t)$$

$$\delta V = \sqrt{\left(\frac{\delta(\Delta x)}{\Delta t}\right)^2 + \left(\frac{\Delta x * \delta(\Delta t)}{(\Delta t)^2}\right)^2} \approx \frac{\delta(\Delta x)}{\Delta t} \quad [2]$$

$$\Delta x = x_f - x_0 \quad [3]$$

$$\delta(\Delta x) = \delta(x_f) - \delta(x_0) \quad [4]$$

To address the latter, it is important to consider the trade-off between using a longer camera gate width and a shorter one. A longer gate will allow more light to reach the aperture, but at the cost of increased error. Typically for longer delays, the time delay used to calculate velocity is simply the time between the arrival of the pulse and the time corresponding to the middle of the exposure gate time interval, as represented by $\delta t = \frac{1}{2}g + d$, where g is the camera gate and d is the delay, assuming that the fluorescence intensity is constant during the exposure time. But when that delay is on the order of microseconds, approaching the exposure time of the camera, the gate width becomes nontrivial with respect to the delay and methods to evaluate the total delay time should be reevaluated. The timing uncertainty here is approximated by adding the camera gate width to the overall timing jitter in the measurement apparatus: $\delta(\Delta t) \approx g + 35$ns. Displacement uncertainty $\delta(\Delta x)$ (Equations 3-4) includes the standard deviation of the fitted Gaussian centers at each pixel location over 200 shots and a 5% fitting error. By using a Gaussian fitting procedure, we can achieve

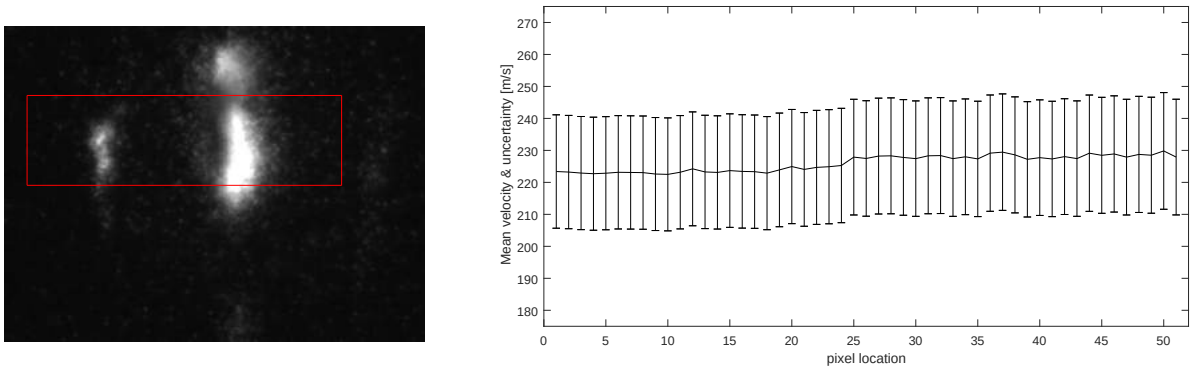

(a) (b)

Figure 10. (a) The velocity fits are taken over the region indicated by the red box and the flow is going from right to left. From right to left, the fluorescent lines taken in burst mode correspond to $t = 0$ and $t = 5$. (b) This plot shows the mean velocity [m/s] and one standard deviation uncertainty computed with Equation 2 using signal lines measured at $t = 0$ and $t = 5\mu s$. Mean velocity is found over 100 shots and uncertainty at each horizontal position reflects the standard deviation over the same dataset. Note that the y-axis (velocity) does not begin at zero.

sub-pixel resolution. Uncertainty is further complicated by the presence of fully-developed turbulent flow at the pipe exit. For a comprehensive analysis, the parameter $\delta(\Delta x)$ must be modified to exclude shot-to-shot displacement uncertainties caused by the flow and not the measurement instrument. Figure 10b depicts the mean velocity uncertainty (top) and mean velocity with error bars representing uncertainty (bottom) for the data taken in the pure R134a turbulent pipe flow, as calculated using Equation 2. This represents an upper bound for the actual measurement precision since it includes variations caused by turbulent flow. No significant difference in velocity uncertainty is found in the R134a + 5% air flow data. A row of fifty pixels, representing approximately 0.9mm at the pipe exit, is fitted. This region indicated by Figure 10a is chosen to maximize the area of usable signal and avoid discontinuous signal regions, as seen previously in Figures 8 and 9. Clumping and signal discontinuity prevent good fits along the entire velocity profile. The uncertainty does not vary significantly across the row of pixels, suggesting that the appearance of "clumps" in the signal does not introduce large errors into the line center fit.

IV. Conclusion

Femtosecond laser velocimetry has been demonstrated in pure R134a flows and R134a flows with small percentages of air between 0.1 atm and 1 atm. A time-resolved pressure dependence in the signal is reflected in changing relative intensities of two peaks in the near-UV spectrum. The pressure dependence of this technique is also manifested in the decrease of overall signal intensity as the pressure increases, although even at atmospheric pressure, the signal may be strong enough for a single-shot measurement, or at least an averaged measurement. A minimum energy of 0.5 mJ per pulse at 800 nm and 1 kHz focused with a f=25 cm lens is necessary to produce a signal lifetime of several microseconds in our gas cell. The signal lifetime increases with increasing power. This technique is shown to be appropriate for measuring mean and instantaneous velocities in a pure R134a flow or in a mixture of R134a with small percentages of air. The single shot precision of this tagging method is demonstrated to be about 18 m/s in a turbulent flow. This non-intrusive and unseeded method should be able to provide quantitative velocity measurements for the TDT facility if practical issues such as optical access and focusing the laser beam through this heavy gas in a large-scale wind tunnel can be addressed.

References

[1]M. H. Barnes, D. Ambur, N. Friend, W.A. Kilgore, D. Valro, and et al. Bisset, B. Ground facilities and testing directorate at nasa langley. NP-2009-06-157-LaRC, 2009.

[2]J. Corliss and S. Cole. Heavy Gas Conversion of the NASA Langley Transonic Dynamics Tunnel. In *20th AIAA Advanced Measurement and Ground Testing Technology Conference*, page 2710, Albuquerque, NM, June 1998.

[3]S. R. Cole, T. E. Noll, and B. Perry. Transonic dynamics tunnel aeroelastic testing in support of aircraft development. *Journal of Aircraft*, 40(5):820–831, 2000.

[4]S. Cole, D. Keller, and D. Piatak. Contributions of the nasa langley transonic dynamics tunnel to launch vehicle and spacecraft development. In *41st Structures, Structural Dynamics, and Materials Conference and Exhibit*, page 1772, Atlanta, GA, April 2000.

[5]B. H. K. Lee, S. J. Price, and Y. S. Wong. Nonlinear aeroelastic analysis of airfoils: bifurcation and chaos. *Progress in aerospace sciences*, (3):205–334, 1999.

[6]M. Karpel. Design for active flutter suppression and gust alleviation using state-space aeroelastic modeling. *Journal of Aircraft*, (3):221–227, 1982.

[7]V. Mukhopadhyay. Transonic flutter suppression control law design and wind-tunnel test results. *Journal of Guidance Control and Dynamics*, (5):930–937, 2000.

[8]T. Liu. *Pressure- and Temperature-Sensitive Paints*. John Wiley & Sons, Ltd, 2005.

[9]A.N. Watkins, B.D. Leighty, W.E. Lipford, D.M. Oglesby, K.Z. Goodman, W.K. Goad, L.R. Goad, and EA. Massey. The development and implementation of a cryogenic pressure sensitive paint system in the national transonic facility. In *47th AIAA Aerospace Sciences Meeting including The New Horizons Forum and Aerospace Exposition*, pages 1–10. American Institute of Aeronautics and Astronautics, 2009.

[10]U. Fey, R. H. Engler, Y. Egami, Y. Iijima, K. Asai, U. Jansen, and J. Quest. Transition detection by temperature sensitive paint at cryogenic temperatures in the european transonic windtunnel (etw). In *20th International Congress on Instrumentation in Aerospace Simulation Facilities (ICIASF)*. German Aerospace Center, 2003.

[11]J. N. Forkey, N. D. Finkelstein, W. R. Lempert, and R. B. Miles. Demonstration and characterization of filtered rayleigh scattering for planar velocity measurements. *AIAA journal*, 34(3):442–448, 1996.

[12]E. B. Cummings. Laser-induced thermal acoustics: simple accurate gas measurements. *Optics Letters*, 19(17):1361–1363, 1994.

[13]L. R. Gartrell, P. B. Gooderum, W. W. Hunter Jr, and J. F. Meyers. Laser velocimetry technique applied to the langley 0.3 meter transonic cryogenic tunnel. *NASA Technical Memorandum*, page 81913, 1981.

[14]Snchez-Gonzlez, Rodrigo Rodney DW Bowersox, and Simon W. North. Simultaneous velocity and temperature measurements in gaseous flow fields using the venom technique. *Optics letters*, 36(2):196–198, 2011.

[15]R. B. Miles, Deyu Zhou, B. Zhang, W. R. Lempert, and Z.S. She. Fundamental turbulence measurements by relief flow tagging. *AIAA Journal*, 31(3):447–452, 1993.

[16]N. M. Sijtsema, N. J. Dam, R. J. H. Klein-Douwel, and J. J. Ter Meulen. Air photolysis and recombination tracking: A new molecular tagging velocimetry scheme. *AIAA Journal*, 40(6):1061–1064, 2002.

[17]J. B. Michael, M. R. Edwards, A. Dogariu, and R. B. Miles. Femtosecond laser electronic excitation tagging for quantitative velocity imaging in air. *Applied Optics*, 50(26):5158–5162, 2011.

[18]Ross A. Burns and Paul M. Danehy. Fleet velocimetry measurements on a transonic airfoil. In *55th AIAA Aerospace Sciences Meeting*, page 0026. American Institute of Aeronautics and Astronautics, 2017.

[19]N. Jiang, B. R. Halls, H. U. Stauffer, P. M. Danehy, J. R. Gord, and S. Roy. Selective two-photon absorptive resonance femtosecond-laser electronic-excitation tagging velocimetry. *Optics Letters*, 41(10):2225–2228, 2016.

[20]N. Jiang, J. G. Mance, M. N. Slipchenko, J. J. Felver, H. U. Stauffer, T.... Yi, and S. Roy. Seedless velocimetry at 100 khz with picosecond-laser electronic-excitation tagging. *Optics Letters*, 42(2):239–242, 2017.

[21]N. Calvert, Y. Zhang, and R. B. Miles. Characterizing FLEET for Aerodynamic Measurements in Various Gas Mixtures and non-Air Environments. In *32nd AIAA Aerodynamic Measurement Technology and Ground Testing Conferenceg*, page 3206, Washington, DC, June 2016.

[22]Y. Zhang, N. Calvert, M. N. Shneider, and R. B. Miles. Enhancement of FLEET in Argon Gas Mixtures. In *32nd AIAA Aerodynamic Measurement Technology and Ground Testing Conferenceg*, page 3249, Washington, DC, June 2016.

[23]Y. Zhang, M. N. Shneider, and R. B. Miles. Characterization of intermediate reactions following femtosecond laser excitation in argon-nitrogen mixtures. In *55th AIAA Aerospace Sciences Meeting*, page 0841, Grapevine, TX, January 2017.

[24]V. M. Apatin, V. O. Kompanets, V. B. Laptev, Y. A. Matveets, E. A. Ryabov, S. V. Chekalin, and V. S. Letokhov. Excitation and dissociation of polyatomic molecules under the action of femtosecond infrared laser pulses. *Russian Journal of Physical Chemistry B*, 1(2):113–119, 2007.

[25]H. Ku. Notes on the use of propagation of error formulas. *J Research of National Bureau of Standards-C. Engineering and Instrumentation*, 70C(4):263–273, 1966.